General Corrosion Behavior and Oxide Film Properties of Alloy 690 Exposed to Four Different Zinc Water Chemistry

Do Haeng Hur [a*], Soon-Hyeok Jeon [a], Dong-Seok Lim [a], Jinsoo Choi [b], Kyu-Min Song [b]
[a] *Nuclear Materials Research Division, Korea Atomic Energy Research Institute, Daejeon 34057*
[b] *Central Research Institute of Korea Hydro & Nuclear Power Co., Ltd., Daejeon 34101*
[*]Corresponding author: dhhur@kaeri.re.kr

1. Introduction

The addition of zinc cations into the reactor coolant is a very effective water chemistry measure to suppress radiation buildup and stress corrosion cracking [1]. The beneficial effects are attributed to changes in properties of the oxides formed on the materials in the zinc-injected coolant. Compared to zinc-free conditions, important observations for oxides formed in zinc water chemistry can be summarized as follows: a decrease in the size and amount of oxide particles in the outer oxide layer [2]; a significant reduction of the oxide film thickness [3]; incorporation of zinc into the oxide films [4]; a decrease of cobalt uptake in the oxide films [5]; and a significant decrease in the corrosion and release rates [6].

The observations mentioned above were obtained from studies using fresh specimens. Zinc cations can be injected into the coolant initially at the startup of a new plant with fresh surfaces on the structural materials. However, many plants have employed zinc addition after a certain period of operation in zinc-free environments. In this case, the effect of application may be different from that of the former case. Therefore, in this study, we report the effect of zinc addition on the corrosion behavior and oxide film properties of Alloy 690 in four different zinc water chemistry of a PWR.

2. Experimental Methods

2.1 Preparation of Test Material

Alloy 690 steam generator tubing was used as a test material, which had been finally heat-treated at 715℃ for 10.6 h. The tubing had nominal dimensions of 19.05 mm outer diameter and 1.07 mm wall thickness.

Tubular pieces 50 mm long were sectioned into half along the tube axial direction to prepare corrosion coupons. The surfaces of the coupons were abraded with silicon carbide paper down to 2000 grit, followed by ultrasonic cleaning in acetone.

2.2 Corrosion Tests and Oxide Characterization

Table I shows four different zinc water chemistry and test conditions: Case #1: exposure to non-zinc water throughout the test for 3000 h; Case #2: exposure to non-zinc water for an initial 1500 h and subsequent exposure to zinc water for 1500 h; Case #3: exposure to zinc water for an initial 1500 h and subsequent exposure to non-zinc water for 1500 h; and Case #4: exposure to zinc water throughout the test for 3000 h.

Corrosion tests were performed using two different circulating water loop systems with and without zinc to avoid zinc contamination. After the tests, the morphologies and chemical compositions of the oxides formed on the coupons were examined using scanning electron microscopy (SEM), energy dispersive X-ray spectroscopy (EDS), and X-ray photoelectron spectroscopy (XPS). Oxidized corrosion coupons were chemically descaled to obtain the corrosion and release rates using the two-step descaling process [7]. The corrosion rate was calculated using the total weight of oxidized base metal, which was obtained through the chemical descaling and gravimetric method.

Space charge capacitance measurements of the oxide films formed under the conditions without zinc (Case #1) and with zinc (Case #4) for 3000 h were performed in a borated buffer solution (0.05 M H_3BO_3 + 0.075 M $Na_2B_4O_7$) at 25℃. The measurements were run at a frequency of 1000 Hz with a 10 mV ac amplitude. The dc potential was applied in the cathodic direction from +1.5 V to –1.5 V vs. the open circuit potential with a potential step of 25 mV.

Table I: Experimental conditions

Four zinc water chemistry		Common
Case #1	3000 h without Zn	2 ppm Li 1000 ppm B DO[1)] < 5 ppb DH[2)]=3.12 ppm 330℃
Case #2	1500 h without Zn→1500 h with 10 ppb Zn	
Case #3	1500 h with 10 ppb Zn→1500 h without Zn	
Case #4	3000 h with 10 ppb Zn	

DO[1)] : dissolved oxygen, DH[2)] : dissolved hydrogen

3. Results and Discussion

3.1 Morphology and Composition of Oxide Films

Fig. 1 shows SEM images of the corrosion coupons after exposure to the four different conditions at 330℃ for 3000 h. In Case #1, the surfaces of the corrosion specimens were completely covered with small, polyhedral particles approximately 100–200 nm in size and consequently the original surface could not be

observed. Large polyhedral particles with a size of approximately 1–3 ㎛ were sparsely distributed on the coated layer. The appearance of the Case #2 specimens was analogous to that of the Case #1 specimens, but the size and number of large crystals decreased. In Cases #3 and #4 exposed initially to zinc, the size and amount of surface particles drastically decreased.

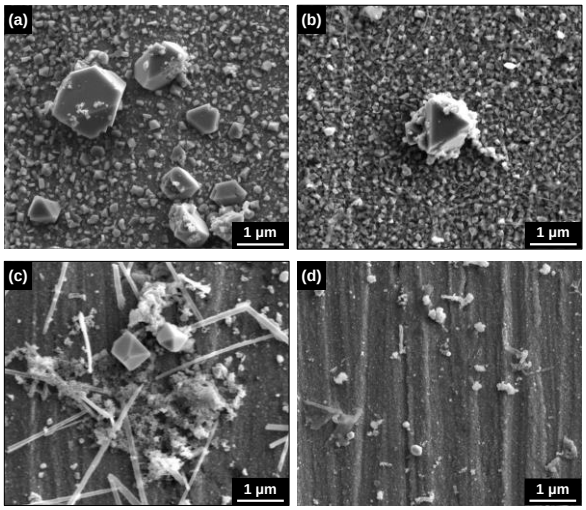

Fig. 1. SEM images of the corrosion coupons after exposure to the four different conditions at 330℃ for 3000 h: (a) Case #1, (b) Case #2, (c) Case #3, and (d) Case #4.

A double-layered oxide was formed on the Alloy 690 coupons regardless of water chemistry. The outer layer was thick and loose, while the inner layer was thin and compact. The outer oxides were mainly composed of nickel, iron and chromium, while the inner oxides were enriched in chromium. Zinc was incorporated in the inner oxide layers when the specimens were exposed to zinc chemistry. The zinc contents of the inner layers increased in the following order: Case #2 < Case #3 < Case #4. Comparing Case #3 with Case #2, it is apparent that more zinc was incorporated in the oxides of the specimen exposed initially to zinc. As shown in Fig. 2, the nickel and iron contents of the inner layers increased in the following order: Case #1 < Case #2 < Case #3 < Case #4, which in turn resulted in a decrease in chromium content in the same order.

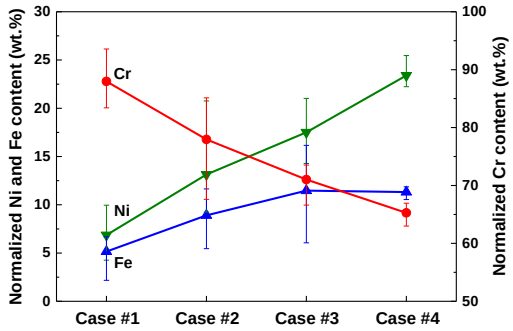

Fig. 2. Normalized chemical compositions of the inner oxide layers formed under the four different zinc water chemistry.

3.2 Corrosion and Release Behavior

Fig. 3 shows the corrosion rates of Alloy 690 under the four different test conditions. The zinc addition resulted in an apparent reduction in the corrosion rates compared to that without zinc addition: The corrosion rate decreased by only 8 % for Case #2, but 25 % for Case #3, and 33 % for Case #4 relative to that for Case #1 without zinc. These results show that the weights of base metals oxidized during the tests were decreased as much by the zinc addition. The corrosion rate of Case #3 was 19 % lower than that of Case #2, indicating that initial exposure to zinc was much more effective than later exposure to zinc water chemistry.

The zinc addition clearly decreased the release rates in a similar trend to the corrosion rates. The release rate decreased by 22 % for Case #2, 43 % for Case #3, and 52 % for Case #4 compared to that for Case #1. The release rate of Case #3 was 27 % lower than that of Case #2, indicating that initial exposure to zinc is much more beneficial.

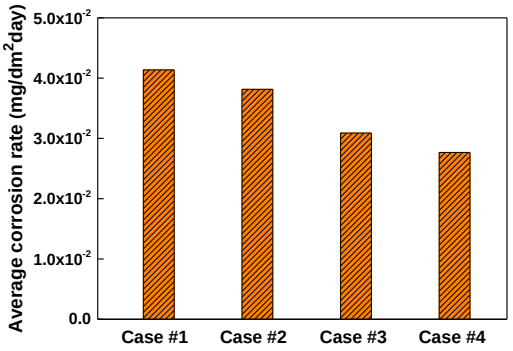

Fig. 3. Average corrosion rates of Alloy 690 under the four different zinc water chemistry.

3.3 Mott-Schottky Analyses of Oxide Films

Fig. 4 shows the capacitance behavior of oxide films formed in the solutions without zinc (Case #1) and with zinc (Case #4) for 3000 h. The capacitance values of oxides formed under the Case #4 condition was significantly smaller than those under Case #1, indicating that the film resistance of Case #4 is much greater than that of Case #1. The capacitance responses of the two oxide films revealed both n-type and p-type semiconducting behavior. The positive slopes in regions I and II are due to an n-type semiconductor, while the negative slopes in regions III and IV represent a p-type semiconducting response. It is well known that chromium oxide and iron oxide behave as a p-type semiconductor and an n-type semiconductor, respectively [8–9]. Therefore, the Mott-Schottky behavior reflected that the oxide films consisted of the chromium-rich inner oxide layer and the outer ferrite-rich oxide layer.

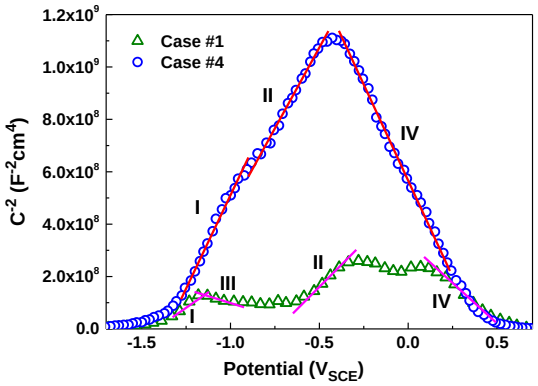

Fig. 4. Mott-Schottky plots of oxides grown on Alloy 690 in solutions without zinc (Case #1) and with zinc (Case #4).

Table II shows the calculated charge carrier densities using the slope of the straight lines and the Mott-Schottky relation [10]. The total donor and acceptor densities in the oxide films of Case #4 were approximately one fifth of those in the films of Case #1. This indicates that the point defect densities in the oxide films declined drastically when the films were formed in zinc water. Point defects in the oxide films are known to provide diffusion paths of metal cations and oxygen anions [11]. Therefore, the significant decrease in the corrosion and release rates are due, in part, to a decrease in the defect concentration in the inner oxide layers grown in zinc water.

Table II: Donor and acceptor densities in oxides calculated by Mott-Schottky analyses

	Region I ($x10^{21}$ cm^{-3})	Region II ($x10^{21}$ cm^{-3})	Region III (10^{21} cm^{-3})	Region IV (10^{21} cm^{-3})
Case #1	16.8	21.8	61.8	18.7
Case #4	7.99	8.83	-	8.16

4. Conclusions

Zinc water chemistry was beneficial for a reduction in the corrosion and release rates of Alloy 690. These benefits are attributed to the zinc-incorporated chromium-rich inner oxide layer. Zinc was incorporated in the pre-oxidized coupons that were subsequently exposed to zinc water, and still remained in the oxides even after cessation of zinc injection, thereby contributing to a reduction in the corrosion and release rates. The oxide morphology, corrosion rate and release rate of Alloy 690 were strongly dependent on the initial water chemistry when the alloy was subsequently exposed to another water chemistry. Therefore, it is best to inject zinc into the primary water at the initial startup of new plants without mature oxide films on the materials.

Acknowledgements

This study was financially supported by the Korea Hydro & Nuclear Power Co., LTD of the Republic of Korea (L18S061000). This work was also supported by the National Research Foundation (NRF) grant funded by the government of the Republic of Korea (NRF-2017M2A8A4015159).

REFERENCES

[1] K. Fruzzetti, Overview Report on Zinc Addition in Pressurized Water Reactors–2004, EPRI, 2004 Palo Alto, CA, USA.
[2] S.E. Ziemniak, H. Hanson, Zinc treatment effects on corrosion behavior of Alloy 600 in high temperature, hydrogenated water, Corros. Sci. 48 (2006) 3330–3348.
[3] X. Liu, X.Wu, E.-H. Han, Effect of zinc injection on established surface oxide films on 316L stainless steel in borated and lithiated high temperature water, Corros. Sci. 65 (2012) 136–144.
[4] J. Huang, X. Liu, E.-H. Han, X. Wu, Influence of Zn on oxide films on Alloy 690 in borated and lithiated high temperature water, Corros. Sci. 53 (2011) 3254–3261.
[5] P.J. Bennett, P. Gunnerud, H. Loner, J.K. Pettersen, A. Harper, The effects of zinc addition on cobalt deposition in PWRs, In Water Chemistry of Nuclear Reactor Systems 7, BNES: Bournemouth, UK, 1996.
[6] J.N. Esposito, G. Economy, W.A. Byers, J.B. Esposito, F.W. Pement, R.J. Jacko, C.A. Bergmann, The addition of zinc to primary reactor coolant for enhanced PWSCC resistance, In Proceedings of the Fifth International Symposium on Environmental Degradation of Materials in Nuclear Power Systems–Water Reactors, Monterey, CA, USA, 25–29 August 1991; American Nuclear Society: La Grange Park, IL, USA; pp. 495–501.
[7] M.J. Seo, H.-S. Shim, K.M. Kim, S.-I. Hong, D.H. Hur, Influence of surface roughness on the corrosion behavior of Alloy690TT in PWR primary water, Nucl. Eng. Des. 280 (2014) 62–68.
[8] N.B. Hakiki, S. Boudin, B. Rondot, M. Da Cunha Belo, The electronic structure of passive films formed on stainless steels, Corros. Sci. 37 (1995) 1809–1822.
[9] F. Gaben, B. Vuillemin, R. Oltra, Influence of the chemical composition and electronic structure of passive films grown on 316L SS on their transient electrochemical behavior, J. Electrochem. Soc. 151 (2004) B595–B604.
[10] N.E. Hakiki, M. Da Cunha Belo, Electronic structure of passive films formed on molybdenum-containing ferritic stainless steels, J. Electrochem. Soc. 143 (1996) 3088−3094.
[11] D.D. Macdonald, The history of the point defect model for the passive state: a brief review of film growth aspects, Electrochim. Acta 56 (2011) 1761–1772.